5-15-2002

Calculations on the size effects of Raman intensities of silicon quantum dots

Wei Cheng
Illinois State University

Shang-Fen Ren
Illinois State University

Calculations on the size effects of Raman intensities of silicon quantum dots

Wei Cheng* and Shang-Fen Ren
Department of Physics, Illinois State University, Normal, Illinois 61790-4560
(Received 7 May 2001; revised manuscript received 13 November 2001; published 25 April 2002)

Raman intensities of Si quantum dots (QD's) with up to 11489 atoms (about 7.6 nm in diameter) for different scattering configurations are calculated. First, phonon modes in these QD's, including all vibration frequencies and vibration amplitudes, are calculated directly from the lattice-dynamic matrix by using a microscopic valence force field model combined with the group theory. Then the Raman intensities of these quantum dots are calculated by using a bond-polarizability approximation. The size effects of the Raman intensity in these QD's are discussed in detail based on these calculations. The calculations are compared with the available experimental observations. We are expecting that our calculations can further stimulate more experimental measurements.

DOI: 10.1103/PhysRevB.65.205305 PACS number(s): 78.30.−j, 63.22.+m, 02.20.−a, 81.05.Cy

I. INTRODUCTION

Semiconductor quantum dots (QD's) have attracted much research attention in recent years because of their importance in the fundamental understanding of physics and potential applications in electronic devices, information processing, and nonlinear optics. The electronic properties of QD's have been intensively studied in recent years, both theoretically and experimentally, and a clear understanding of much of the basic physics of the quantum confinement effects of electrons in QD's has been achieved.[1] On the other hand, the vibration properties of QD's, i.e., the confinement of phonon modes in QD's, are less understood.

So far, most of the theoretical understanding of phonon modes in QD's is based on the continuum dielectric models. The analytic expression of the eigenfunctions of LO phonons and surface optical phonons of small spherical[2–10] and cylindrical[11] QD's has been derived and the electron-phonon interactions calculated. The extended continuum dielectric model[8–10] coupling the mechanical vibrational amplitudes and the electrostatic potential has made major improvements over classical dielectric models in the study of phonon modes in QD's. However, one of the basic assumptions of all dielectric models is that the material is homogeneous and isotropic, that is, only valid in the long-wavelength limit. When the size of QD's is small, in the range of a few nanometers, the continuum dielectric models are intrinsically limited.

Many optical, transport, and thermal properties of quantum dots are related to phonon behavior in QD's. The theoretical treatment of these properties requires a reliable description of phonon modes and electron-phonon interaction potential in QD's. One of the major difficulties of the microscopic modeling of phonon modes in QD's is its computational intensity. For example, a GaAs QD of size of about 8.0 nm contains 11 855 atoms. Considering the three-dimensional motion of each atom, the dynamic matrix is in the order of 35 565. This is an intimidating task even with the most advanced computers. In recent years, we have developed a microscopic valence force field model[12–15] (VFFM) to study phonon modes in QD's by employing the projection operators of the irreducible representations of the group theory to reduce the computational intensity. By employing the group theory, for example, the above matrix of size of 35 565 can be reduced to five matrices in five different representations of A_1, A_2, E, T_1, and T_2, with the sizes of 1592, 1368, 2960, 4335, and 4560, respectively. Therefore, the original problem is reduced to a problem that can be easily handled by most reasonable computers. This allows not only the investigation of phonon modes in QD's with a much larger size, but also the investigation of phonon modes in QD's with different symmetries. These investigations lead to many interesting physics that otherwise cannot be revealed.[12–15] With this model, we have studied the size effects of phonon modes in semiconductor quantum dots, including QD's of one material, such as GaAs or InAs, as well as QD's with a core of one material embedded in a shell of another material, such as GaAs cores embedded in AlAs shells. To further develop our theoretical model in investigations of properties of QD's, in this paper, we have studied the size effects of Raman intensity in semiconductor QD's with the same model.

It is well known that the measurement of Raman spectra of crystals is one of the most important methods for obtaining information about their lattice vibrations.[16,17] Raman spectroscopy has been used to investigate the geometry, the nature, and the structures of QD's.[2,3,18–22] So far, most of the theoretical calculations on Raman scattering are based on the phenomenological model.[2,3] Recently there have been calculations based on microscopic models,[25,26] but because of the limitation on the computational intensity, the size range of the QD's that can be handled is limited.

In this paper, we have calculated the Raman intensities of nanoscale Si QD's by using the results of the VFFM together with a bond-polarizability approximation (BPA).[23–28] The calculated results are then compared with the available experimental data. We also hope that our calculations can further stimulate more experimental measurements on Raman intensities of semiconductor QD's.

The paper is organized as follows. In Sec. II, we describe the theoretical models of the VFFM and BPA; in Sec. III, we show our calculated results of Raman intensities and have some discussions; and Sec. IV is a summary.

II. THEORETICAL APPROACHES

A. VFFM for phonon modes in QD's

In general, the theoretical model, VFFM, that we used to investigate phonon modes in QD's can be used to study phonon modes in group IV, III-V, and II-VI semiconductors. In this model, the change of the total energy due to the lattice vibration is considered as two parts, the change of the energy due to the short-range interactions and the change of the energy due to the long-range Coulomb interaction:

$$\Delta E = \Delta E_s + \Delta E_c , \tag{2.1}$$

where the short-range interaction describes the covalent bonding, and the long-range part approximates the Coulomb interactions of polar semiconductor compounds. For the short-range part, we employed a VFFM with only two parameters as the following:[29]

$$\Delta E_s = \sum_i \tfrac{1}{2} C_0 \left(\frac{\Delta d_i}{d_i} \right)^2 + \sum_j \tfrac{1}{2} C_1 (\Delta \theta_j)^2, \tag{2.2}$$

where C_0 and C_1 are two parameters describing the energy change due to the bond-length change and the bond angle change, respectively. The summation runs over all the bond lengths and bond angles. Because each of these two parameters has a simple and clear physical meaning, this model allows us to treat the interaction between atoms near and at the surface appropriately. It can be further used to treat the effects of surface relaxations and reconstructions on the vibrations if necessary. The parameters C_0, C_1 used in our calculations for Si are 49.1 and 1.07 eV, respectively.[29] Since silicon is a homopolar semiconductor in which all atoms are neutral, the long-range Coulomb interaction[30] is not necessary.

When considering the interaction between atoms, special attention is paid to atoms near the surfaces of the QD's. More specifically, for the short-range interaction, when an atom is located near the surface, interaction from its nearest-neighboring atom is considered only if that specific nearest atom is within the QD, and interaction from its second-neighboring atom is considered only if that specific second-neighbor atom is in the QD as well as the nearest-neighboring atom that makes the link between them. The second point is important, because it makes sense with the physics meanings of these two parameters, but it is easy to be neglected.

As we discussed in the above section, we have employed the projection operators of the irreducible representations of the group theory to reduce the computational intensity[31–34] when calculating phonon modes directly from the dynamic matrices. When the results of phonon modes are used to calculate the Raman intensity of QD's, the advantage of applying the group theory to calculate phonon modes in different symmetries is even more obvious. Because of the symmetry dependence of Raman intensity, only phonon modes that are Raman active in that specific symmetry are necessary to be considered. This further reduces the amount of calculations required.

B. Bond-polarizability approximation

With the vibrational normal modes obtained from the VFFM described, we use the BPA (Ref. 23) to calculate Raman-scattering intensity of QD's. This BPA model was used in the prediction of Raman intensities of semiconductor superlattices,[24–26] fullerences,[27] and nanotubes.[28]

The BPA (Ref. 23) associates an axially symmetric polarizability tensor with each bond as

$$\vec{\vec{P}}(\vec{R}_{ij}) = \alpha(R_{ij})\vec{\vec{I}} + \gamma(R_{ij})\left[\hat{R}_{ij}\hat{R}_{ij} - \frac{1}{3}\vec{\vec{I}} \right], \tag{2.3}$$

where $\vec{\vec{I}}$ is a unit matrix, $\alpha(R_{ij})$ is the mean polarizability, and $\gamma(R_{ij})$ describes the anisotropy of the polarizability. Both $\alpha(R_{ij})$ and $\gamma(R_{ij})$ are functions of the bond length R_{ij} and not direction dependent. Here $\vec{R}_{ij}$ is the bond vector connecting atoms i and j, R_{ij} is the length of $\vec{R}_{ij}$, and $\hat{R}_{ij} = \vec{R}_{ij}/R_{ij}$. With phonon vibrations we have $\vec{R}_{ij} = \vec{r}_{ij} + \vec{u}_{ij} = \vec{r}_{ij} + \vec{u}_j - \vec{u}_i$, where $\vec{r}_{ij}$ is the bond vector at equilibrium, $\vec{u}_i$ is the displacement of atom i, and $\vec{u}_{ij}$ is the relative displacement of atoms j and i. For phonon vibrations, the condition that $\vec{u}_{ij} \ll \vec{r}_{ij}$ always applies. Therefore, the polaribility tensor $\vec{\vec{P}}(\vec{R}_{ij})$ can be expressed in powers of the displacements $\vec{u}_{ij}$ in a Taylor's expansion. The constant term of this expansion, i.e., $\vec{\vec{P}}(\vec{r}_{ij})$, can be ignored, since the total contribution of this term from all bonds to the Raman intensity vanishes. Keeping the first order of $\vec{u}_{ij}$ in the Taylor's expansion, the polarizability tensor $\vec{\vec{P}}(\vec{R}_{ij})$ can be simplified as the following:

$$\begin{aligned} \vec{\vec{P}}(\vec{R}_{ij}) \approx & (\vec{u}_{ij} \cdot \hat{r}_{ij})[\alpha'(r_{ij})\vec{\vec{I}} + \gamma'(r_{ij})(\hat{r}_{ij}\hat{r}_{ij} - \tfrac{1}{3}\vec{\vec{I}})] \\ & + r_{ij}^{-1}\gamma(r_{ij})[\vec{u}_{ij}\hat{r}_{ij} + \hat{r}_{ij}\vec{u}_{ij} - 2(\vec{u}_{ij} \cdot \hat{r}_{ij})\hat{r}_{ij}\hat{r}_{ij}], \end{aligned} \tag{2.4}$$

where $\alpha'(r_{ij})$ and $\gamma'(r_{ij})$ are derivatives of $\alpha(\vec{R}_{ij})$ and $\gamma(\vec{R}_{ij})$ with respect to $\vec{u}_{ij}$ evaluated at the equivalent bond vector $\vec{r}_{ij}$, respectively, and $\hat{r}_{ij} = \vec{r}_{ij}/r_{ij}$.

In the zinc-blende structure, there are four different bond orientations, so we only need to calculate $\vec{\vec{P}}(\vec{R}_{ij})$ for these four different types of bonds. We can choose the following four directions as the bond orientations:

$$\hat{r}_{01} = \frac{1}{\sqrt{3}}(1,-1,1),$$

$$\hat{r}_{02} = \frac{1}{\sqrt{3}}(-1,1,1),$$

$$\hat{r}_{03} = \frac{1}{\sqrt{3}}(1,1,-1),$$

$$\hat{r}_{04} = \frac{1}{\sqrt{3}}(-1,-1,-1), \tag{2.5}$$

and the four polarizations associated with the four bonds are

$$\overleftrightarrow{P}(\vec{R}_{01})=\frac{1}{\sqrt{3}}(u_{01,x}-u_{01,y}+u_{01,z})\left[\alpha'\begin{pmatrix}1&0&0\\0&1&0\\0&0&1\end{pmatrix}+\frac{1}{3}\gamma'\begin{pmatrix}0&-1&1\\-1&0&-1\\1&-1&0\end{pmatrix}\right]$$
$$+\frac{\gamma}{3\sqrt{3}}\begin{pmatrix}4u_{01,x}+2u_{01,y}-2u_{01,z}&-u_{01,x}+u_{01,y}+2u_{01,z}&u_{01,x}+2u_{01,y}+u_{01,z}\\-u_{01,x}+u_{01,y}+2u_{01,z}&-2u_{01,x}-4u_{01,y}-2u_{01,z}&2u_{01,x}+u_{01,y}-u_{01,z}\\u_{01,x}+2u_{01,y}+u_{01,z}&2u_{01,x}+u_{01,y}-u_{01,z}&-2u_{01,x}+2u_{01,y}+4u_{01,z}\end{pmatrix}, \tag{2.6}$$

$$\overleftrightarrow{P}(\vec{R}_{02})=\frac{1}{\sqrt{3}}(-u_{02,x}+u_{02,y}+u_{02,z})\left[\alpha'\begin{pmatrix}1&0&0\\0&1&0\\0&0&1\end{pmatrix}+\frac{1}{3}\gamma'\begin{pmatrix}0&-1&-1\\-1&0&1\\-1&1&0\end{pmatrix}\right]$$
$$+\frac{\gamma}{3\sqrt{3}}\begin{pmatrix}-4u_{02,x}-2u_{02,y}-2u_{02,z}&u_{02,x}-u_{02,y}+2u_{02,z}&u_{02,x}+2u_{02,y}-u_{02,z}\\u_{02,x}-u_{02,y}+2u_{02,z}&2u_{02,x}+4u_{02,y}-2u_{02,z}&2u_{02,x}+u_{02,y}+u_{02,z}\\u_{02,x}+2u_{02,y}-u_{02,z}&2u_{02,x}+u_{02,y}+u_{02,z}&2u_{02,x}-2u_{02,y}+4u_{02,z}\end{pmatrix}, \tag{2.7}$$

$$\overleftrightarrow{P}(\vec{R}_{03})=\frac{1}{\sqrt{3}}(u_{03,x}+u_{03,y}-u_{03,z})\left[\alpha'\begin{pmatrix}1&0&0\\0&1&0\\0&0&1\end{pmatrix}+\frac{1}{3}\gamma'\begin{pmatrix}0&1&-1\\1&0&-1\\-1&-1&0\end{pmatrix}\right]$$
$$+\frac{\gamma}{3\sqrt{3}}\begin{pmatrix}4u_{03,x}-2u_{03,y}+2u_{03,z}&u_{03,x}+u_{03,y}+2u_{03,z}&-u_{03,x}+2u_{03,y}+u_{03,z}\\u_{03,x}+u_{03,y}+2u_{03,z}&-2u_{03,x}+4u_{03,y}+2u_{03,z}&2u_{03,x}-u_{03,y}+u_{03,z}\\-u_{03,x}+2u_{03,y}+u_{03,z}&2u_{03,x}-u_{03,y}+u_{03,z}&-2u_{03,x}-2u_{03,y}-4u_{03,z}\end{pmatrix}, \tag{2.8}$$

$$\overleftrightarrow{P}(\vec{R}_{04})=\frac{1}{\sqrt{3}}(-u_{04,x}-u_{04,y}-u_{04,z})\left[\alpha'\begin{pmatrix}1&0&0\\0&1&0\\0&0&1\end{pmatrix}+\frac{1}{3}\gamma'\begin{pmatrix}0&1&1\\1&0&1\\1&1&0\end{pmatrix}\right]$$
$$+\frac{\gamma}{3\sqrt{3}}\begin{pmatrix}-4u_{04,x}+2u_{04,y}+2u_{04,z}&-u_{04,x}-u_{04,y}+2u_{04,z}&-u_{04,x}+2u_{04,y}-u_{04,z}\\-u_{04,x}-u_{04,y}+2u_{04,z}&2u_{04,x}-4u_{04,y}+2u_{04,z}&2u_{04,x}-u_{04,y}-u_{04,z}\\-u_{04,x}+2u_{04,y}-u_{04,z}&2u_{04,x}-u_{04,y}-u_{04,z}&2u_{04,x}+2u_{04,y}-4u_{04,z}\end{pmatrix}. \tag{2.9}$$

When we calculate the polarizability tensor for the QD's, we sum the polarizability tensor associated with each bond in the QD's, and get a scattering tensor

$$\overleftrightarrow{P}=\sum_{i<j}\overleftrightarrow{P}(\vec{R}_{ij}). \tag{2.10}$$

From the symmetry property, we know that the Raman tensor in cubic crystals takes the following forms:[35]

$$\overleftrightarrow{P}_{A1}=\begin{pmatrix}a&0&0\\0&a&0\\0&0&a\end{pmatrix}, \tag{2.11}$$

$$\overleftrightarrow{P}_{E}=\begin{pmatrix}b&0&0\\0&b&0\\0&0&-2b\end{pmatrix},\quad\begin{pmatrix}\sqrt{3}b&0&0\\0&-\sqrt{3}b&0\\0&0&0\end{pmatrix}, \tag{2.12}$$

$$\overleftrightarrow{P}_{T2}=\begin{pmatrix}0&0&0\\0&0&d\\0&d&0\end{pmatrix},\quad\begin{pmatrix}0&0&d\\0&0&0\\d&0&0\end{pmatrix},\quad\begin{pmatrix}0&d&0\\d&0&0\\0&0&0\end{pmatrix}. \tag{2.13}$$

In our calculations we found that for semiconductor QD's with a zinc-blende structure, after we applied the projection operators, $\overleftrightarrow{P}$ is a constant times a unit matrix for an A_1 mode, a traceless diagonal matrix with two equal matrix elements for an E mode, and a traceless matrix with only nondiagonal

matrix elements for a T_2 mode. The Raman tensors $\overleftrightarrow{P}$ for the QD's can be expressed in the following forms:

$$\overleftrightarrow{P}_{A1}=\begin{pmatrix} A_l & 0 & 0 \\ 0 & A_l & 0 \\ 0 & 0 & A_l \end{pmatrix}, \tag{2.14}$$

$$\overleftrightarrow{P}_{E}=\begin{pmatrix} 2E_l & 0 & 0 \\ 0 & -E_l & 0 \\ 0 & 0 & -E_l \end{pmatrix}, \tag{2.15}$$

$$\overleftrightarrow{P}_{T2}=\begin{pmatrix} 0 & 0 & 0 \\ 0 & 0 & T_l \\ 0 & T_l & 0 \end{pmatrix}, \tag{2.16}$$

where

$$A_l^2=[(P_{11}^l+P_{22}^l+P_{33}^l)/3]^2, \tag{2.17}$$

$$E_l^2=\tfrac{1}{18}[(P_{11}^l-P_{22}^l)^2+(P_{22}^l-P_{33}^l)^2+(P_{33}^l-P_{11}^l)^2], \tag{2.18}$$

and

$$T_l^2=[(P_{12}^l)^2+(P_{23}^l)^2+(P_{31}^l)^2], \tag{2.19}$$

where P_{ij}^l is the element of the change of the polarizability resulting from vibration of the QD's in mode l as defined in Eq. (2.10).

The A_l^2, E_l^2, and T_l^2 are invariants of the Raman tensor and l is an index of the modes. This is consistent with the Raman tensor in cubic crystals of above [Eqs. (2.11)–(2.13)]. Here A_l^2 is related to the intensity of an A_1 mode in polarized Raman geometry, and E_l^2 and T_l^2 are related to intensities of E and T_2 modes in depolarized Raman geometry, respectively. For E or T_2 modes that are two or threefold degenerate, the contributions of the degeneracies are considered in the total scattering intensity.[16,17]

For unpolarized incident light with frequency Ω scattered perpendicular to the direction of propagation, the intensities of Raman-scattered components with frequencies $\Omega\pm\omega_l$ are the following:[23]

$$I_{||}=\frac{(\overline{n_l}+\frac{1}{2}\pm\frac{1}{2})}{2\omega_l}g(\omega_l)[7G_l^2+45A_l^2], \tag{2.20}$$

$$I_{\perp}=\frac{(\overline{n_l}+\frac{1}{2}\pm\frac{1}{2})}{2\omega_l}g(\omega_l)[6G_l^2], \tag{2.21}$$

where $\overline{n_l}$ is the average occupation number of phonon mode l, and $I_{||}$ and $I_{\perp}$ are intensities of scattered light with polarization parallel and perpendicular to the plane of scattering. In these equations, A_l^2 is the same as defined in Eq. (2.17), and

$$G_l^2=9E_l^2+3T_l^2. \tag{2.22}$$

The Raman-scattering matrix for cubic crystals with arbitrary orientations and arbitrary incident and scattering light wave vectors are studied by using Stokes vectors.[36] The Stokes vectors are defined as the following:

Let the incident elliptic polarization be described as

$$\vec{E}=(a+ib)\vec{E}_A+(c+id)\vec{E}_N, \tag{2.23}$$

where $\vec{E}_A$ and $\vec{E}_N$ are polarization vectors in and normal to the scattering plane. These two directions are labeled as $\vec{A}$ and $\vec{N}$, respectively. The Stokes vector is defined as

$$\begin{pmatrix} a^2+b^2+c^2+d^2 \\ a^2+b^2-c^2-d^2 \\ 2(ac+bd) \\ 2(ad-bc) \end{pmatrix}. \tag{2.24}$$

For example, for a left-handed circularly polarized light viewed along the direction of propagation of the light, its polarization vector is $\vec{E}=(1/\sqrt{2})\ (i\vec{E}_A+\vec{E}_N)$, and its equivalent Stokes vector is (1, 0, 0, −1). From this, the Stokes parameters of the scattering light are derived choosing four different combinations of values of a, b, c, and d. This gives the complete scattering matrix a_{ij}. Assuming that QD's orient randomly, all the possible incident directions should be averaged. Then the scattering matrix for A_1 modes is[36]

$$a_{ij}=\begin{pmatrix} 1+\cos^2\Theta & -1+\cos^2\Theta & 0 & 0 \\ -1+\cos^2\Theta & 1+\cos^2\Theta & 0 & 0 \\ 0 & 0 & 2\cos\Theta & 0 \\ 0 & 0 & 0 & 2\cos\Theta \end{pmatrix}, \tag{2.25}$$

and for both E and T_2 modes it is

$$a_{ij}=\begin{pmatrix} 13+\cos^2\Theta & -1+\cos^2\Theta & 0 & 0 \\ -1+\cos^2\Theta & 1+\cos^2\Theta & 0 & 0 \\ 0 & 0 & 2\cos\Theta & 0 \\ 0 & 0 & 0 & -10\cos\Theta \end{pmatrix}, \tag{2.26}$$

where Θ is the scattering angle.

In our calculations, we have calculated A_l^2, $9E_l^2$, and $3T_l^2$ according to the right-angle scattering Eqs. (2.20)–(2.22). For different incident light and scattering configurations, the Raman intensities are the linear combination of these three according to their Stokes vectors.

III. RESULTS AND DISCUSSION

In this paper we report calculated reduced Raman-scattering intensity, $\omega_l I/(\overline{n_l}+\frac{1}{2}\pm\frac{1}{2})$, for Si QD's with diameters from 15 to 76 Å. Since α', $r_{ij}^{-1}\gamma$, and γ' are not accurately known *a priori*, these parameters used in our calculations satisfy[23]

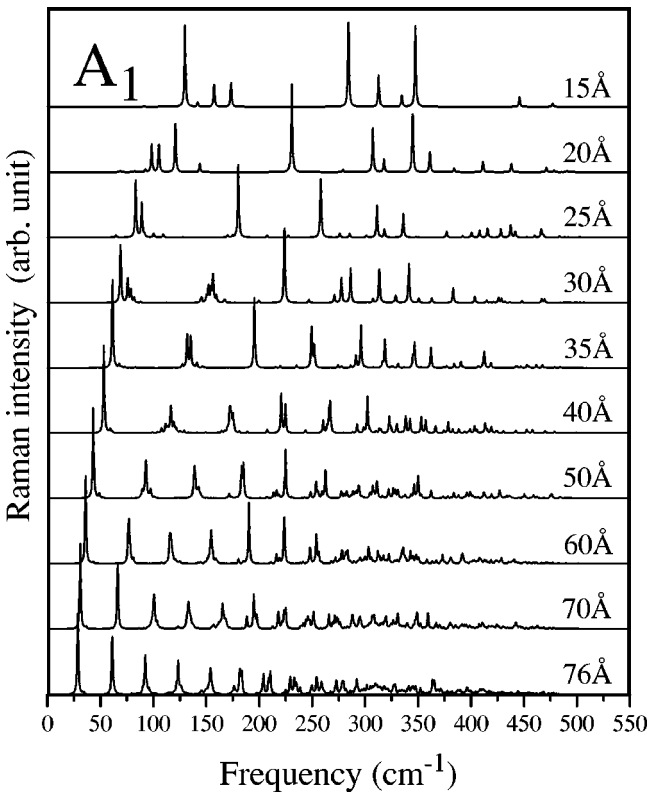

FIG. 1. Reduced Raman intensities of A_1 modes for Si QD's with approximate diameters in angstrom indicated.

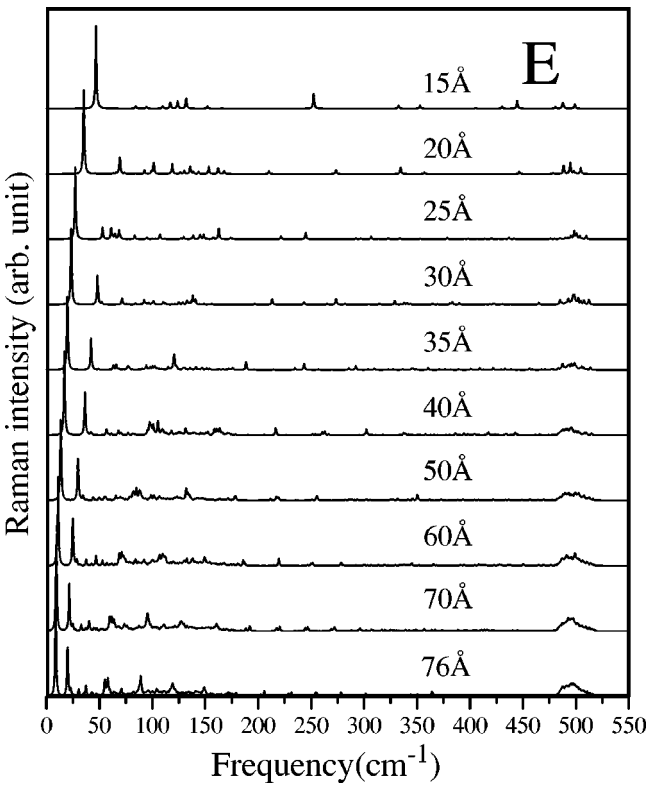

FIG. 2. Reduced Raman intensities of E modes for Si QD's with approximate diameters in angstrom indicated.

$$r_{ij}^{-1}\gamma(r_{ij})=\tfrac{3}{8}\gamma'(r_{ij})=\tfrac{3}{8}\alpha'(r_{ij}). \tag{3.1}$$

We noticed that in the early calculations of amorphous Si,[23] $\alpha'\simeq 0$ was assigned because the observed intensity profiles $I_{\parallel}$ and $I_{\perp}$ of Si have the same shape. If $\alpha'=0$, there would be no contribution to Raman intensity from A_1 modes. However, when the size of QD's is small, the contribution from A_1 modes might be important to consider, so we have assigned α' a number as above. The choice of this number is not critical, since for different choices of α', the shape of Raman intensity from the A_1 contribution is the same, and only its relevant strength to E and T_2 modes is different.

We have calculated Raman intensities of A_1, E, and T_2 modes for Si QD's with approximate sizes of 15, 20, 25, 30, 35, 40, 50, 60, 70, and 76 Å, respectively, and the results are shown in Figs. 1–3. Here the Raman intensity I is calculated by the Lorentz broadening

$$I=\sum_l \frac{I_l\Gamma/\pi}{(\Gamma)^2+(\omega-\omega_l)^2}, \tag{3.2}$$

where I_l and ω_l are the scattering intensity and eigenfrequency of mode l, respectively, and Γ is the half Lorentz width, which is taken as $2/\pi=0.64\ \mathrm{cm}^{-1}$ in our calculations. We have also listed the related important data in Table I that are numerically more clear. The data listed in Table I in order are the diameters of the QD's calculated (d), the number of atoms in the QD's (N), the intensity of the highest peak of A_1 modes (I_{A1}), the intensity of the highest peak of E modes (I_E), the intensity of the highest peak of T_2 modes in the low-frequency range $[I_{T2}(l)]$ and in the high-frequency range $[I_{T2}(h)]$, the frequency of the first peak of A_1 modes (ω_{A1}), the frequency of the first peak of E modes (ω_E), the frequency of the first peak of T_2 modes in the low-frequency range $[\omega_{T2}(l)]$, and the frequency of the highest peak of T_2 modes in the high-frequency range $[\omega_{T2}(h)]$. All the intensities listed above are Raman intensity per atom for easier comparison. We will discuss the important features of these results in detail next.

A. Size effects of highest frequencies

From Figs. 1–3 we see that in general, the major peaks in the high-frequency range always have T_2 symmetry. The highest peaks correspond to T_2 phonon modes with the highest frequencies. When the size of the QD's increases, this frequency approaches the frequency of the optical-phonon frequency of bulk Si. Theoretically speaking, when the size of QD's approaches infinity, the total Raman spectrum of QD's approaches the Raman spectrum of bulk Si, and this will be the only peak left.

In our previous calculations of phonon modes in QD's,[12–15] we have discussed the size dependence of phonon modes with different symmetries. We have learned that phonon modes with different symmetries have different size dependence, and A_1 modes usually have the strongest size effect. For quantum dots of zinc-blende semiconductors, such

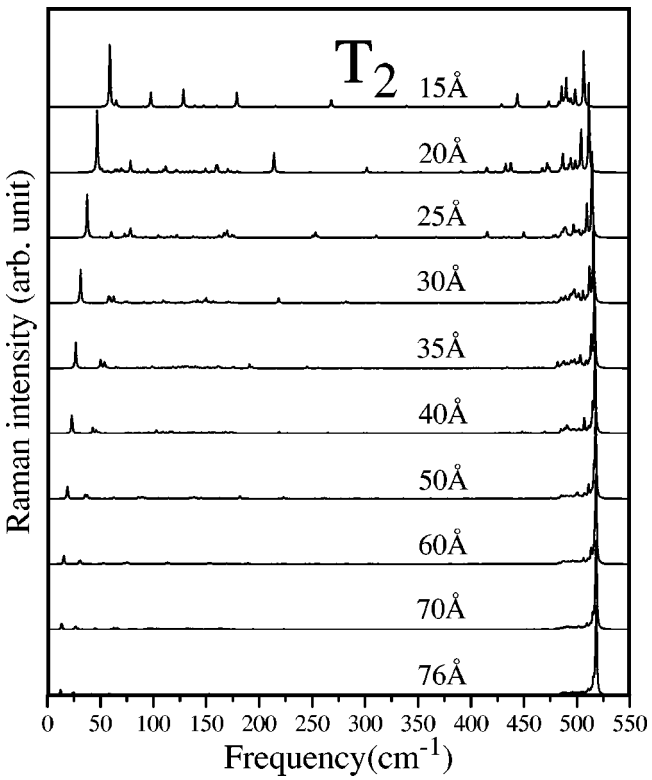

FIG. 3. Reduced Raman intensities of T_2 modes for Si QD's with approximate diameters in angstrom indicated.

as GaAs, when the size of QD's is large, the mode with the highest frequency has A_1 symmetry. However, as the dot size decreases, there is a crossover of the symmetries, and then the mode with the highest frequency has T_2 symmetry. For Si quantum dots studied in the present paper, the mode with the highest frequency is always of A_1 symmetry. However, the Raman intensity of A_1 modes decreases when the dot size increases, so the strongest high-frequency mode is always of T_2 symmetry.

When the size of QD's decreases, the frequency of this T_2 peak decreases. To show this more clearly, we enlarged the high-frequency range of Fig. 3 and plotted it as Fig. 4. From the data listed in Table I, we know that when the diameter of Si QD's decreases from 75.79 Å to 14.11 Å, the frequency of the highest Raman peak shifts from 518.3 cm^{-1} to 506.4 cm^{-1} (the Raman peak of bulk Si is at 518.9 cm^{-1} in our model). The systematic redshift of the longitudinal (LO) phonon peaks due to spatially confined phonon modes in nanocrystals in the size range of a few nanometers has been observed,[19–21] and recently it has been observed by resonant Raman scattering in three samples of Ge nanocrystals in the size range of 4–10 nm.[18] One more thing we notice from Fig. 3 and Fig. 4 for the high-frequency peaks of T_2 modes is that not only do the highest intensity peak redshifts occur as dot size decreases, but also weaker peaks appear at the same time.

Experimentally it may be difficult to resolve all the weaker peaks because of broadening resulting from fluctuation in dot sizes. As a result one may observe an asymmetric broadening of the Raman peak corresponding to the optical phonon as the dot size is reduced. This is indeed found in Raman intensities of Ge QD's.[37] One may attempt to intepret this as an indication that the quality of the dots may be poorer leading to larger inhomogeneous broadening as the dot size gets smaller. However, from our calculations on Raman intensities of QD's, one can notice that the redshift of the strongest T_2 Raman peak is smaller than the frequency spread of the weaker peaks which appear. In other words the broadening of the Raman peak is larger than the redshift as the dot size decreases. This indicates that the observed broadening in Raman measurements is not only due to the

TABLE I. Raman intensities of A_1, E, and T_2 modes for Si QD's with approximate sizes of 15, 20, 25, 30, 35, 40, 50, 60, 70, and 76 Å. The data listed in order are the diameters of the QD's (d), the number of atoms in the QD's (N), the intensity of the highest peak of A_1 modes (I_{A1}), the intensity of the highest peak of E modes (I_E), the intensity of the highest peak of T_2 modes in the low-frequency range [$I_{T2}(l)$], the intensity of the highest peak of T_2 modes in the high-frequency range [$I_{T2}(h)$], the frequency of the first peak of A_1 modes (ω_{A1}), the frequency of the first peak of E modes (ω_E), the frequency of the first peak of T_2 modes in the low-frequency range [$\omega_{T2}(l)$], and the frequency of the highest peak of T_2 modes in the high-frequency range [$\omega_{T2}(h)$]. All the intensities listed here are Raman intensity per atom.

d	N	I_{A1}	I_E	$I_{T2}(l)$	$I_{T2}(h)$	ω_{A1}	ω_E	$\omega_{T2}(l)$	$\omega_{T2}(h)$
14.11	87	7.65	9.70	10.99	9.88	129.8	46.7	58.8	506.4
19.39	191	5.88	5.58	6.61	9.60	98.4	35.2	46.9	511.2
24.74	417	3.55	3.53	4.79	9.47	83.3	27.2	37.5	514.3
29.75	705	2.69	2.76	3.66	9.22	69.0	23.3	31.2	515.6
34.67	1099	2.46	2.03	2.64	9.25	61.4	19.7	26.6	516.5
39.91	1707	1.84	1.51	1.97	9.24	53.2	16.9	22.9	517.1
50.00	3265	1.27	1.01	1.34	9.47	43.2	13.4	18.8	517.7
59.99	5707	0.91	0.72	0.93	9.67	36.0	10.9	15.5	518.1
69.97	9041	0.68	0.54	0.69	10.04	30.9	9.2	13.4	518.3
75.79	11489	0.58	0.46	0.59	10.26	28.6	8.6	12.4	518.3

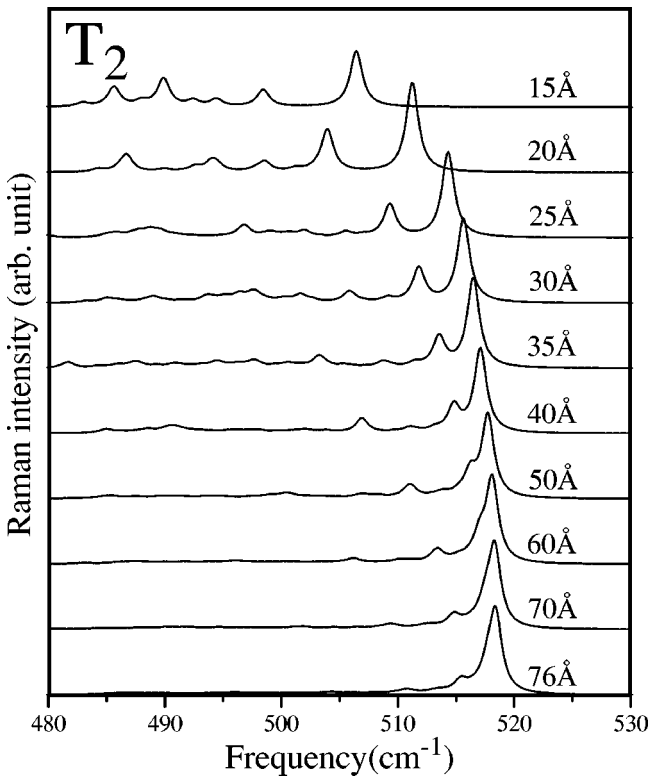

FIG. 4. Reduced Raman intensities of T_2 modes enlarged at the high-frequency range for Si QD's with approximate diameters in angstrom indicated.

redshift of the peak alone, but there is also a contribution to this broadening from quantum size effects.

B. Size effects of lowest frequencies

From Figs. 1–3, we see that the frequency of the first peak in the low-frequency range for all three different symmetries (A_1, E, and T_2) increases as the size of the QD's decreases. From the data listed in Table I, we see that when the size of Si QD's decreases from 75.79 Å to 14.11 Å, the frequency of the first Raman peak of A_1 modes shifts from 28.6 cm^{-1} to 129.8 cm^{-1}, the first Raman peak of E modes shifts from 8.6 cm^{-1} to 46.7 cm^{-1}, and the first Raman peak with T_2 symmetry shifts from 12.4 cm^{-1} to 58.8 cm^{-1}. The size effects of lowest frequencies of phonon modes in QD's have been discussed in detail in our previous studies,[12–15] and again this is shown in the calculated Raman spectra. Furthermore, we notice that even though the frequencies of the lowest-frequency peak increase in all these three figures, they increase at a different rate. The lowest-frequency of the A_1 peak increases much faster than that of the other two. To show this more clearly, we plot the lowest frequency peaks versus the sizes of QD's in Fig. 5. It is obvious that the lowest frequency of the A_1 peak increases much faster than that of the other two, because the A_1 modes have the strongest quantum confinement effects.[12,13]

Another feature of Fig. 5 is that the lowest frequencies of the Raman peaks in the acoustic range are roughly proportional to the inverse of the QD diameters, which was observed by Duval.[2] This was recently observed in Si nanocrystals,[38] and it was noticed that the depolarized Raman spectra appear at much lower frequencies than the polarized ones. Not only do our results agree with the experimental observations, but we also learned that this is actually due to the symmetry dependence of the confinement effect of phonon modes, i.e., the A_1 modes have the strongest confinement effects.

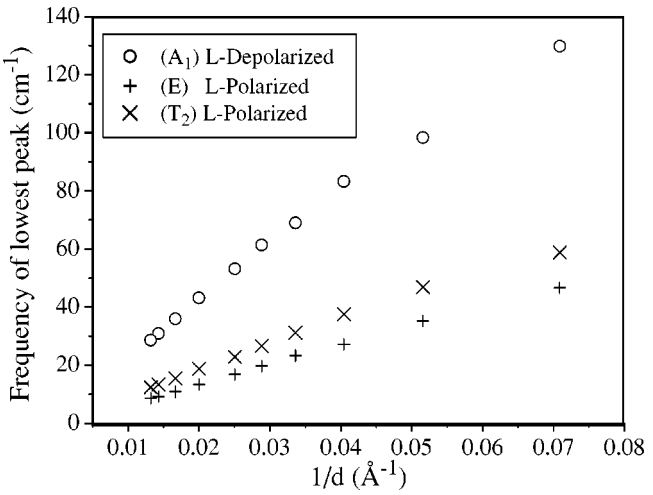

FIG. 5. Frequency of the lowest Raman peak of A_1, E, and T_2 modes versus size of the dots for Si QD's.

C. Folding of the acoustic phonons

In Fig. 1, we see that at the low-frequency range of the A_1 modes, the Raman spectra are dominated by a series of nearly evenly spaced peaks in the acoustical phonon range. As the size decreases, the spacing increases. This can be understood from the folding of acoustic phonons. Since the A_1 modes vibrate in the radical direction, when the radius of the QD's increases approximately one lattice constant, there will be one more folding due to the confinement of the QD's along the radial direction. This should be observable by Raman scattering, and we are expecting such observations.

D. Size effects on strength of Raman peaks

Since Raman intensities plotted in Figs. 1 –3 are in arbitrary units, the size effects on the strength of Raman peaks are not shown clearly in these figures. To show them more clearly, we have plotted the Raman intensity per atom versus diameters of QD's for the low-frequency A_1 peaks, the low-frequency E peaks, the low-frequency T_2 peaks, and the high-frequency T_2 peaks in Fig. 6. For A_1 Raman spectra there are several high peaks, and we choose the strength of the highest peak (when the size is less than 30 Å, this peak is not the peak with the lowest frequency). In Fig. 6 we see that the strength of low-frequency peaks (A_1, E, and T_2) decreases quickly as the size of QD's increases, and the strength of high-frequency peaks (T_2) remains a constant in QD's of all sizes. This indicates that even though in bulk material only one major peak can be measured, when the size of QD's decreases, other peaks in the low-frequency range

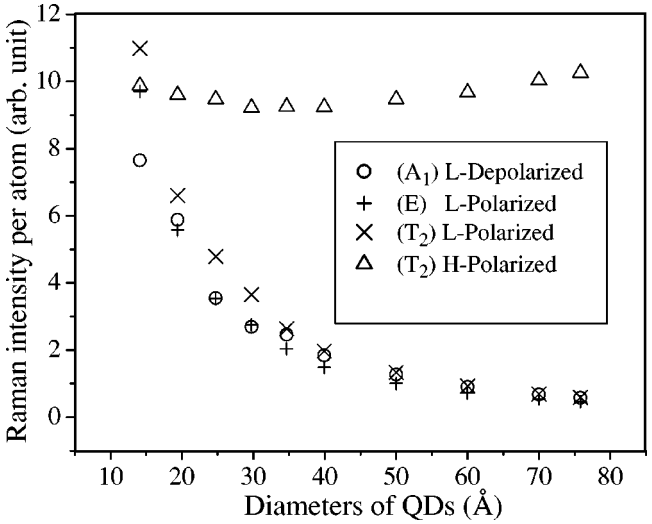

FIG. 6. Raman intensity per atom of the highest low-frequency peaks of A_1, E, and T_2 modes and the highest high-frequency peaks of T_2 modes versus size of the dots for Si QD's.

will appear. Of these low-frequency Raman peaks, the most noticeable ones are probably the evenly spaced A_1 peaks in the polarized spectra. Such evenly spaced A_1 peaks should be observable.

We want to emphasize that in Fig. 6, the Raman intensity shown is from one calculated highest Raman peak, either in the low-frequency range or in the high-frequency range. Experimentally the presence of multiple Raman peaks as shown in Figs. 1–4 may not be resolvable due to size fluctuation, and instead a broadened peak is observed. Typically in such a situation all the Raman intensity should be integrated to obtain the total strength of the Raman peak. To compare with the experimental results, we summed the calculated Raman intensities (without broadening) for all A_1, E, and T_2 modes, respectively, and show them for QD's with different sizes in Fig. 7. We can see that all the Raman intensities will increase when the size of QD's gets smaller. When the QD's get larger, the Raman intensity of T_2 modes will approach the Raman intensity of bulk crystal and others will approach zero. This is in qualitative agreement with what was observed in Ge QD's.[37]

E. Size effects on mode mixing

One more thing we want to comment on from Figs. 1–3 and Fig. 6 is that for large size QD's, the major peak of the Raman spectra is derived from the T_2 high-frequency mode. This peak approaches the optical-phonon peak in the bulk Raman spectra when the size of QD's is large. When the size of QD's decreases, more and stronger peaks at the lower-frequency range appear, which are derived from the A_1 modes in the polarized Raman spectra and E and T_2 modes from the depolarized Raman spectra. As can be seen from Figs. 1–3 and Fig. 6, the intensities of the A_1, E, and T_2 modes are of nearly the same magnitude for small dots, which indicates the mode mixing due to the quantum confinement of phonon modes in small QD's.

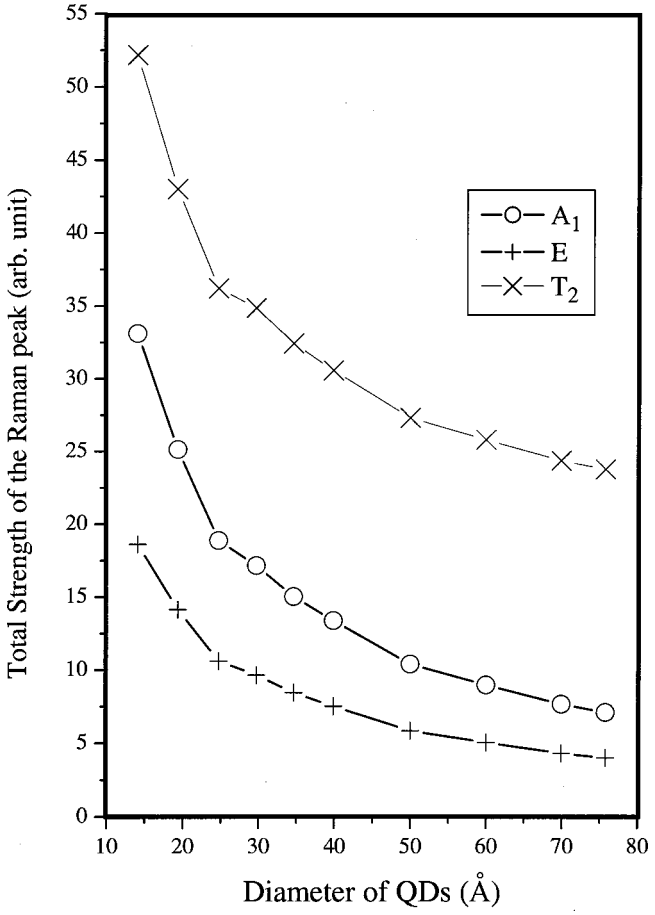

FIG. 7. Integrated Raman intensity per atom of A_1, E, and T_2 modes versus size of the dots for Si QD's.

IV. SUMMARY

In summary, we have calculated the Raman intensities of Si QD's with up to 11 489 atoms (about 7.6 nm in diameter). The phonon modes are calculated directly from the lattice-dynamic matrix of a microscopic VFFM by employing the projection operators of the irreducible representations. Based on the results of phonon modes, the Raman intensities are calculated by using a BPA. The size effects of the Raman intensity in QD's are discussed in detail based on these calculations. Our calculated results agree with the existing experimental observations, and we are expecting that our calculations will stimulate more experimental measurements of Raman intensities of QD's.

ACKNOWLEDGMENTS

This research is supported by the National Science Foundation (Grant Nos. DMR9803005 and INT0001313). We thank Professors Shang-Yuan Ren and Bang-Fen Zhu for helpful discussions. We want to thank Professor Peter Yu for helpful comments that provided us the experimental details on Ge QD's and pointed us further in the direction of comparing our calculated results with the experimental observations. W. Cheng is grateful to Illinois State University for hosting his visit.

*On leave from the Institute of Low Energy Nuclear Physics, Beijing Normal University, Beijing, 100875, P. R. China.
[1] A.D. Yoffe, Adv. Phys. **42**, 173 (1993); **50**, 1 (2001).
[2] E. Duval, Phys. Rev. B **46**, 5795 (1992).
[3] M.C. Klein, F. Hache, D. Ricard, and C. Flytzanis, Phys. Rev. B **42**, 11 123 (1990).
[4] H. Frohlich, *Theory of Dielectrics, Dielectric Constants, and Dielectric Loss* (Oxford University Press, New York, 1949).
[5] R. Fuchs and K.L. Kliewer, Phys. Rev. A **140**, A2076 (1965).
[6] R. Ruppin and R. Englman, Rep. Prog. Phys. **33**, 144 (1970).
[7] C. Trallero-Giner, F. Garcia-Moliner, V.R. Velasco, and M. Cardona, Phys. Rev. B **45**, 11 944 (1992).
[8] E. Roca, C. Trallero-Giner, and M. Cardona, Phys. Rev. B **49**, 13 704 (1994).
[9] M.P. Chamberlain, C. Trallero-Giner, and M. Cardona, Phys. Rev. B **51**, 1680 (1995).
[10] C. Trallero-Giner, A. Debernardi, M. Cardona, E. Menendez-Proupin, and A.I. Ekimov, Phys. Rev. B **57**, 4664 (1998).
[11] W.S. Li and C.Y. Chen, Physica B **229**, 375 (1997).
[12] S.F. Ren, Z.Q. Gu, and D.Y. Lu, Solid State Commun. **113**, 273 (2000).
[13] S.F. Ren, D.Y. Lu, and G. Qin, Phys. Rev. B **63**, 195315 (2001).
[14] G. Qin and S.F. Ren, J. Appl. Phys. **89(11)**, 6037 (2001).
[15] G. Qin and S.F. Ren, Solid State Commun **121,** 171 (2002).
[16] R. Loudon, Proc. R. Soc. London **275**, 218 (1963).
[17] R. Loudon, Adv. Phys. **13**, 423 (1964); **14**, 621 (1965).
[18] K.L. Teo, S.H. Kwok, P.Y. Yu, and S. Guha, Phys. Rev. B **62**, 1584 (2000).
[19] P.T.C. Freire, M.A. Araujo Silva, V.C.S. Reynoso, A.R. Vaz, and V.L. Lemos, Phys. Rev. B **55**, 6743 (1997).
[20] Y.N. Hwang, S. Shin, H.L. Park, S.H. Park, U. Kim, H.S. Jeong, E.J. Shin, and D. Kim, Phys. Rev. B **54**, 15 120 (1996).
[21] A. Balandin, K.L. Wang, N. Kouklin, and S. Bandyopadhyay, Appl. Phys. Lett. **76**, 137 (2000).
[22] G. Armelles, T. Utzmeier, P.A. Postigo, F. Briones, J.C. Ferrer, P. Peiro, and A. Cornet, J. Appl. Phys. **81**, 6339 (1997).
[23] R.J. Bell, in *Methods in Computational Physics*, edited by B. Alder, S. Fernbach, and M. Rotenberg (Academic, New York, 1976), Vol. 15, p. 260.
[24] B.F. Zhu and K.A. Chao, Phys. Rev. B **36**, 4906 (1987).
[25] J. Zi, H. Buscher, C. Falter, W. Ludwig, K. Zhang, and X. Xie, Appl. Phys. Lett. **69**, 200 (1996).
[26] J. Zi, K. Zhang, and X. Xie, Phys. Rev. B **58**, 6712 (1998).
[27] S. Guha, J. Menendez, J.B. Page, and G.B. Adams, Phys. Rev. B **53**, 13 106 (1996).
[28] R. Saito, T. Takeya, and T. Kimura, G. Dresselhaus, and M.S. Dresselhaus, Phys. Rev. B **57**, 4145 (1998).
[29] W.A. Harrison, *Electronic Structure and the Properties of Solids* (Freeman, San Francisico, 1980).
[30] K. Kunc, M. Balkanski, and M.A. Nusimovici, Phys. Status Solidi B **72**, 229 (1975); K. Kunc, Ann. Phys. (Paris) **8**, 319 (1973).
[31] S.Y. Ren, Phys. Rev. B **55**, 4665 (1997).
[32] S.Y. Ren, Solid State Commun. **102**, 479 (1997).
[33] S.Y. Ren, Jpn. J. Appl. Phys., Part 1 **36**, 3941 (1997).
[34] S.Y. Ren and S.F. Ren, J. Phys. Chem. Solids **59**, 1327 (1998).
[35] P. Yu and M. Cardona, *Fundamentals of Semiconductors, Physics and Materials Properties* (Springer, Berlin, 1996).
[36] V. Chandrasekharan, Z. Phys. **175**, 63 (1963).
[37] P. Yu (private communication).
[38] M. Fujii, Y. Kanzawa, S. Hayashi, and K. Yamamoto, Phys. Rev. B **54**, R8373 (1996).